Journal of the Australian Ceramic Society (2026) 62:47–56
https://doi.org/10.1007/s41779-025-01233-9

RESEARCH

Production and characterization of alumina doped sheep and synthetic hydroxyapatite bioinks

Nermin Demirkol[1] · **Aysu Akilli Ari**[2] · **Hatice Evlen**[3]

Received: 21 February 2025 / Revised: 14 June 2025 / Accepted: 25 June 2025 / Published online: 1 July 2025
© The Author(s) 2025

Abstract

This study presents the formulation and evaluation of composite bioinks incorporating synthetic hydroxyapatite (CSHA), sheep-derived hydroxyapatite (SHA), and alumina (Al_2O_3) for extrusion-based 3D bioprinting of bone scaffolds. Rheological analyses demonstrated shear-thinning behavior, with both CSHA/Al_2O_3 and SHA/Al_2O_3 exhibiting comparable viscosity profiles between 400 and 1000 s^{-1}, indicating their suitability for stable extrusion. The bone scaffolds were fabricated using a single-syringe extrusion-based bioprinter. After the printing process, the scaffolds were dried and then immersed in simulated body fluid (SBF) to evaluate their in vitro bioactivity. This immersion process was carried out under static conditions at 36.5 °C for 28 days. SEM and EDS analyses revealed denser apatite nucleation on CSHA/Al_2O_3 scaffolds (Ca/P = 1.33) compared to SHA/Al_2O_3 (Ca/P = 0.88), confirming enhanced bioactivity. FTIR analysis detected characteristic phosphate and carbonate bands indicative of bone-like apatite formation. Cell viability and cytocompatibility were assessed using MTT and WST-1 assays with L929 fibroblasts and osteoblasts. While fibroblast viability showed no significant difference ($p > 0.05$), CSHA/Al_2O_3 scaffolds promoted significantly higher osteoblast viability ($p < 0.05$). Confocal microscopy confirmed sustained osteoblast proliferation at 36 h. These findings demonstrate that CSHA/Al_2O_3-based bioinks possess favorable printability, mineralization potential, and osteogenic support, making them strong candidates for future bone tissue engineering applications using ceramic-reinforced bioprinting strategies.

Keywords 3D bioprinting · Alumina · Hydroxyapatite · Bone scaffold · Cell culture

Introduction

When considering the importance of bones in the human body, bone diseases and injuries become a significant concern. Congenital diseases as well as cancers, traumas, osteomalacia or rickets, osteomyelitis, infections, and fractures can lead to damages causing loss of bone tissue and functions [1]. Despite being a dynamic tissue naturally capable of regeneration, this self-renewal and healing capacity is usually sufficient only for the recovery of minor injuries like cracks and certain types of fractures. Reconstruction of bone defects larger than a certain threshold (typically > 2 cm, depending on the anatomical location) often relies on treatments requiring the use of external devices and elements [2, 3]. According to published statistics, it is estimated that half a million patients require bone supplementation each year in the United States and.

Europe alone, with the global cost of bone fractures estimated at 5.5 billion USD annually. The total annual cost of bone repair worldwide is estimated at 17 billion USD [4].

Fixation of bones using inert metallic implants, autografts, and allografts is a crucial process for large bone defects, and such operations are widely performed globally [5]. However, autografts may pose certain limitations and serious risk factors.

Additionally, in the case of allografts, there is also a risk of disease transmission. In this context, there has been a tendency towards the use of designed bone scaffolds, which has progressively increased over time [5, 6]. According to data from the German Federal Statistical Office, in 2008, autografts were used in 74.1% of surgeries requiring bone

✉ Nermin Demirkol
nermin.demirkol@kocaeli.edu.tr

[1] Faculty of Fine Arts, Kocaeli University, Kocaeli, Turkey

[2] Department of Mechanical and Metal Technology, Amasya University, Amasya, Turkey

[3] Faculty of Engineering, Karabuk University, Karabuk, Turkey

replacement, implant allografts in 14.1%, and biomaterials replacing bone in 11.8% of cases.

By 2018, the number of surgeries performed had increased by 15.7%, with autografts, allografts, and biomaterials accounting for 54.9%, 21.3%, and 23.9% of the market share, respectively. This represents a 134.4% increase in the general use of biomaterials as substitutes for bone, with ceramics accounting for 51.2%, bone cement for 38.2%, and synthetic or natural polymers containing other biomaterials for 10.6% of materials used in 2008, while in 2018, these figures reached 41.9%, 37.1%, and 21%, respectively [7].

In recent years, bone tissue engineering has emerged as a new treatment that can assist bone regeneration and overcome limitations of other common methods. The goal of bone tissue engineering is to design materials that can be placed in bone defects and replace the regeneration process with the patient's own tissue until bone repair is achieved. These materials are typically prepared in the form of scaffolds that serve as supportive structures for cellular activity and temporarily play the role of extracellular matrix (ECM) until bone repair occurs [8]. Depending on the defect location and the patient's health condition, the designed system needs to have different structural and functional properties to be useful. Bone scaffolds should provide the desired chemical and physical properties and their mechanical strength should be as similar as possible to that of bone [8, 9]. After implantation into the body, the scaffold initiates a growth process from the surrounding areas towards the interior, and in order for the growth process to continue, it must have open and interconnected pores [10]. An important aspect in bone tissue engineering is that the scaffold materials should degrade at a rate proportional to the rate of bone formation to maintain the stability of the scaffold-bone system and allow bone growth [11]. A scaffold with too rapid degradation rate may collapse its porous structure, impeding mass transfer and leading to tissue necrosis. Conversely, too slow degradation may result in the formation of fibrous capsules and lack of integration with host tissue, making tissue regeneration difficult. Therefore, optimal scaffold degradation kinetics are important in promoting tissue regeneration [12]. Scaffold degradation in the human body is typically a complex, multiscale process that depends on biochemical, physical, geometric, and mechanical factors. This arises from the unique kinetics of degradation/absorption that conform to the specific characteristics of extracellular matrices and different cell types in each patient. Age, nutritional status, underlying diseases, lifestyle, gender, and related factors are variables that affect patients' regenerative capacity and subsequently the required scaffold degradation rate [13]. Various studies have shown that scaffold degradation can be adjusted by manipulating various factors such as material composition, environmental factors (e.g., physical loading), manufacturing method, scaffold structure, and surface properties [14]. Timely degradation of implanted biomaterials is believed to be a crucial factor for successful tissue regeneration.

In this regard, several bone tissue scaffold production methods and biomaterials have been developed to understand and control this process. Three-dimensional bioprinting is one of the most practical methods used to create and develop accurate bone scaffold structures.

Three-dimensional bioprinting has emerged as an interesting technology due to its ability to mimic natural tissue architecture using different cell types and biomaterials [15]. Studies on artificial bone tissue produced by 3D bioprinting method using various mechanical structures and properties with biomaterials have become widespread. With these biomaterials, scaffold structures resembling bone tissues have been created [16].

Ceramics used in bone tissue engineering include the family of calcium phosphates, such as tricalcium phosphate (β-TCP) and hydroxyapatite (HA), magnesium phosphates, magnesium silicates, and calcium silicates [17]. HA, a synthetic biomaterial, is produced from both artificial and living bone. Due to its unique properties, HA nanomaterials and nanocomposites are used in various advanced catalytic technologies and fields [18]. HA is widely used as a biocompatible ceramic in many fields such as orthopedics and dentistry. When implanted in defective areas of bone due to its similarity to bone, it has been found to promote new bone formation [19, 20]. Biocompatible and bioactive composite scaffolds are essential in bone tissue regeneration due to their bioactivity and multilevel porous structures [21]. Therefore, the use of HA biomaterial for the production of porous bone structures has been the right choice.

Alumina (Al_2O_3) has various applications due to its low toxicity to eukaryotic cells, making it a desired biomaterial [22]. Al_2O_3 is a ceramic material with great potential for use as a biomaterial in bone implants [23]. In recent years, interest has increased in materials with high thermal and chemical resistance, as well as in a Al_2O_3 content and optical properties [24].

Alginate is indeed a natural polysaccharide derived from seaweed. It is commonly used in various biomedical applications due to its biocompatibility, rheological properties, and ability to form hydrogels through ionic crosslinking with divalent cations such as calcium ions. This makes it a popular choice as a biomaterial ink for applications such as 3D bioprinting and tissue engineering.

Biomaterial ink holds a significant position in 3D printing. It is crucial for the fluid biomaterial ink to maintain its shape during printing, ensuring that the geometric accuracy of the created layers remains intact and that the pore sizes can be maintained at the desired values. Material compositions

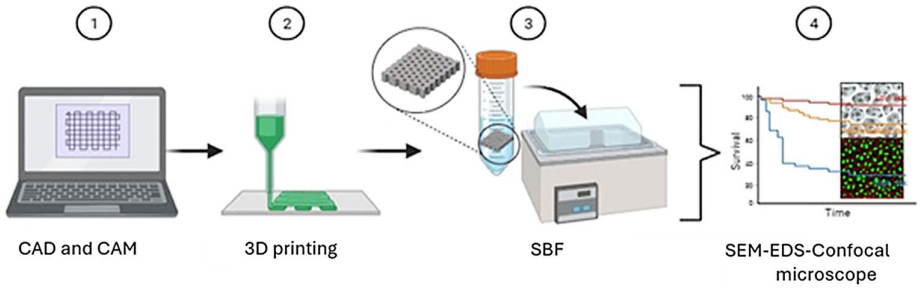


Fig. 1 Bone scaffold experimental stages

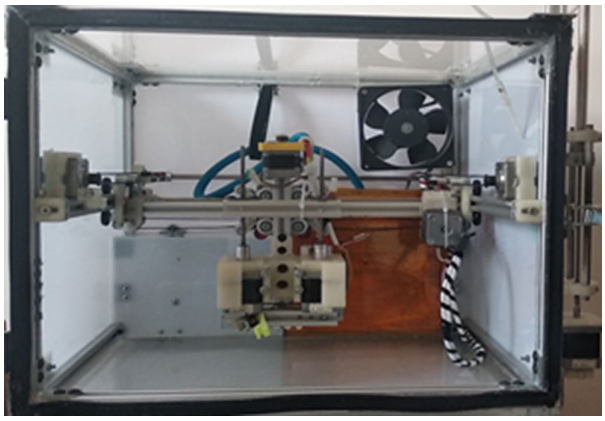


Fig. 2 Single-syringe bioprinter

were formulated taking this aspect into account during the preparation of biomaterial ink.

In this study, bioink was produced with a mixture of HA, Al_2O_3, sodium alginate and pure water. Bone scaffolds were printed with a 3D bioprinter. To investigate its biocompatibility, bone scaffolds were kept in artificial body fluid for four weeks, SEM results were extracted, and cell culture analyses were performed. The stages of scaffold production and examination are schematically illustrated in Fig. 1.

Materials and methods

Materials

Synthetic hydroxyapatite (CSHA) and sheep-derived hydroxyapatite (SHA) were selected as the principal bioceramic components for scaffold fabrication. To enhance both mechanical integrity and biological interaction, alumina (Al_2O_3) was incorporated as a reinforcing phase. CSHA (purity ≥ 99.5%, particle size: 40–50 µm) and Al_2O_3 (purity ≥ 99.5%, particle size: 1–10 µm) were purchased from Nanograph Nano Technology, Ankara, Türkiye. SHA was prepared in-house at Kocaeli University using calcination and grinding processes applied to cleaned ovine bone tissue, resulting in particles with an average diameter of ~10 µm [25]. Sodium alginate ($(C_6H_7NaO_6)_n$, analytical grade) was acquired from Alfasol Chemicals, İstanbul, Türkiye, and used to modulate viscosity and mprove printability. Distilled water (resistivity > 18 MΩ·cm) was used as the solvent in all mixtures to ensure chemical purity. All materials were used without additional purification. Detailed preparation procedures and bioink compositions are described in the following section.

Methods

In bioprinting, the pore size of the scaffold is crucial, and it should ideally be in the range of 100–500 µm to closely mimic the structure of real bone [26, 27]. Achieving pore sizes within this range is an important parameter for bioprinter design.

One of the most important features of the bioprinter designed and produced in this study is its ability to create scaffold voids in microns. This feature affects the scaffold's ability to hold cells during cell culture [28]. A single syringe was used for scaffold printing in the manufactured bioprinter. Step motors were used for syringe pressure and X, Y, Z movements. Plexiglas sheets were used for the cabin's sealability. Sterilization was achieved using UV light in the cabin environment. Fig. 2 shows the design of the bioprinter.

In the study, Al_2O_3 was added to SHA and CSHA matrix materials at a concentration of 10% by weight. Alginate was used to increase the viscosity of these prepared mixtures. The weight ratios of biomaterials used in the biomaterial ink are given in Table 1. These mixtures were mixed at 60 °C using a magnetic stirrer at 500 rpm until the desired viscosity of approximately between 0,03 and 2 mPa·s was reached as measured by a rotational viscometer [29–31]. Once the mixture reached the desired consistency, the biomaterial ink was allowed to cool. It was then loaded into a syringe for printing bone scaffolds. Fig. 3 illustrates the schematic representation of the biomaterial ink preparation steps.

The viscosity of the prepared biomaterial inks was determined through rheology tests conducted using Malvern/Gemini II rheometer device. Rheology experiments were performed at 25 °C temperature using a 4° cone and a 40 mm diameter parallel plate. Measurements were taken

Table 1 Biomaterial ink codes and material mixture ratios

Bioink Codes	Biomaterials	Mixture content [w/v] %
CSHA/Al_2O_3	[CSHA + 10 wt% Al_2O_3+$(C_6H_7NaO_6)_n$]	7.4 [w/v] %, [CSHA + 10 wt% Al_2O_3] 3.8 [w/v] %, [$(C_6H_7NaO_6)_n$] 25 [mL] distilled water
SHA/Al_2O_3	[SHA + 10 wt% Al_2O_3 +$(C_6H_7NaO_6)_n$]	7.4 [w/v] %, [SHA + 10 wt% Al_2O_3] 3.8 [w/v] %, [$(C_6H_7NaO_6)_n$] 25 [mL] distilled water

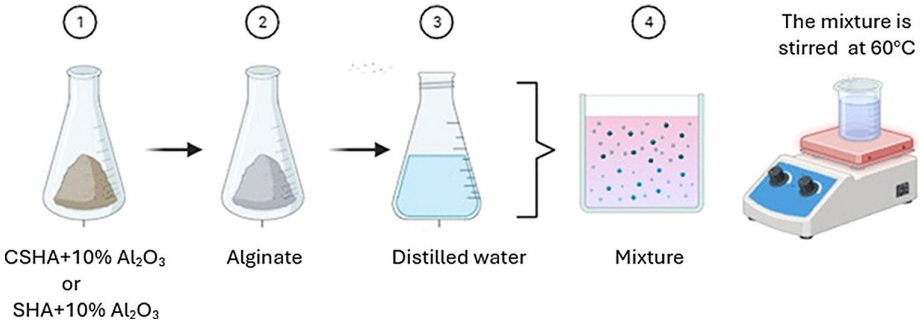


Fig. 3 Stages of biomaterial ink preparation



Fig. 4 Image of bone scaffold

at shear rates ranging from 0.000 to 1000.000 1/s and at a frequency of 1.5 Hz.

Bone scaffold samples with dimensions of 10 × 10 × 0.5 mm were modeled using Computer-Aided Design (CAD) software. The model file was sliced according to 3D printer printing parameters in slicing software (syringe speed 6.67 mm/s, layer thickness 0.25 mm, syringe diameter 0.41 μm) and G-codes were generated with Computer Aided Manufacturing (CAM) software. The model was then printed using the bioprinter. Fig. 4 illustrates the image of the bone scaffold printed via bioprinting.

To observe the bioactivity of the bone tissue scaffolds produced by bioprinting, samples were immersed in artificial body fluid for testing. The artificial body fluid (SBF) was prepared by adding 750 ml of distilled water to a one-liter beaker. The SBF chemicals were added to the distilled water in the specified amounts [32]. After all the materials were added, the solution was brought up to one liter. The temperature of the solution was maintained at 36.5 °C, and the pH value was adjusted.

to 7.14. Subsequently, the solution was transferred to HDPE containers. The bone scaffolds were then immersed in the containers, and the SBF solution was.

renewed daily. The bone scaffolds were kept in the SBF at a temperature of 37 °C for 28 days.

To examine the morphology and topography of.

the produced bone scaffolds, SEM (Scanning Electron Microscopy) and EDS (Energy Dispersive Spectroscopy) analyses were conducted using a scanning electron microscope (Nova NanoSEM 450) FTIR (Fourier Transform Infrared Spectroscopy) analyses were performed on the accumulations collected from the inside of the container of the bone scaffolds extracted from SBF (Simulated Body Fluid) to differentiate different types of clay minerals and obtain information about their structure, composition, and properties. FTIR analyses were applied at Kocaeli University.

For the quantitative evaluation of cell attachment and proliferation on the surface of the bone scaffolds, the MTT (3-(4,5-dimethylthiazol-2-yl)-2,5-diphenyltetrazolium bromide) enzymatic method was employed. The MTT test assesses cellular metabolic activity by measuring the reduced enzyme activity in the mitochondria of living cells. The viability of cells on the printed bone scaffolds was analyzed at HUBTUAM. The "TS EN ISO 10993-5 /October-2010- Annex C MTT Cytotoxicity Test" method was used for quantitative evaluation. L929 and Osteoblast cell lines were used for cell viability analysis. The bone scaffolds were incubated in a 10% cell culture medium at 37 °C with agitation at 50 rpm for 24 h for extraction. The extracts obtained after extraction were used within 24 h. All data were determined as mean ± standard deviation (SD), and

statistical analysis was performed using one-way analysis of variance (ANOVA) to test for significance.

WST-1 Cytotoxicity/Cell viability analyses were conducted using the L929 Mouse Fibroblast cell line. These analyses were performed at the Kocaeli University Stem Cell Center using a Leica DMI SP8 Confocal microscope. The frozen cells were thawed in a water bath at 37 °C after being frozen at -152 °C. The cells were then transferred to a clean medium and centrifuged. The supernatant was then discarded. Cell counting was performed using Trypan Blue and a light microscope. For WST analysis, 20,000 cells were added to each sample, and calculations were made. The bone scaffolds were placed in wells, and cell seeding was performed with complete medium (basal medium containing 10% FBS and 1% Pen/Strep). After the designated time, the culture medium in the wells was removed. Then, basal medium containing 10% WST was added, and incubation was carried out in the dark in an incubator for 12–36 h. After incubation, measurements were taken at a wavelength of 450 nm using spectrophotometers from each well. Absorbance measurement values and graphs related to cell count were then generated using standard wells.

Experimental results

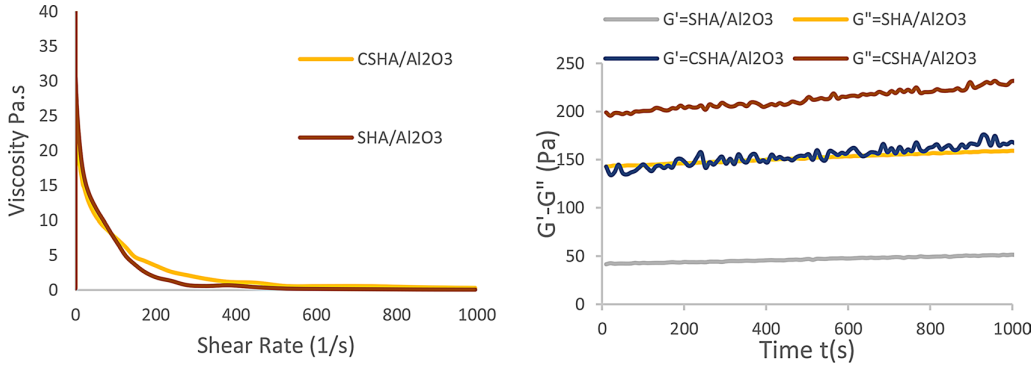
To extrude the bone scaffold and apply pressure, it is necessary to determine the rheological values of the biomaterial. This rheological analysis provides the storage modulus (G') and loss modulus (G") of the biomaterial. Fig. 5 (a) illustrates the relationship between viscosity (Pa.s) and shear rate (1/s) as a function of shear rate for the biomaterial ink.

During the printing of the biomaterial ink, low shear rate and high viscosity are required. In the viscosity-shear rate graph of the prepared biomaterial inks, it is observed that as the shear rate increases within the 0–350 s time interval, the viscosity ratio decreases progressively. Shear-thinning behavior is crucial for bioinks to ensure smooth extrusion and shape fidelity. A low yield stress and linear viscoelastic region within 0–5% strain indicates that the ink can transition from unstable to stable flow without breaking during printing [33]. Upon examination of the graph, it is observed that CSHA/Al_2O_3 and SHA/Al_2O_3 biomaterial inks exhibit similar rheological behavior between shear rates of 400 (1/s) and 1000 (1/s).

In Fig. 5 (b), G' represents the storage modulus and G" represents the loss modulus. When comparing the values of G' and G" with each other, it is observed that the loss modulus is greater than the storage modulus (G" > G'), indicating that no gelation occurs and the material exhibits viscous behavior. Upon examination of the graph, at 600s, the values of viscous behaviors are shown to be CSHA/Al_2O_3 (G"=216.17, G'=160.29) and SHA/Al_2O_3 (G"=153.3, G'=47.605).

To create a bone structure, it is essential to have apatites, which are components of bone. Therefore, the formation of apatites in the prepared scaffolds needs to be investigated by soaking them in SBF. Hence, CSHA/ Al_2O_3 and SHA/ Al_2O_3 bone scaffolds were examined for the formation of apatites by SEM after being soaked in SBF. Fig. 6 compares the SEM images of bone scaffolds taken immediately after 3D printing and after being soaked in SBF for 28 days.

After being soaked in SBF for 28 days, SEM images were taken to check for apatite formation on the surfaces of CSHA/ $Al_2O_3$and SHA/ Al_2O_3bone scaffolds. Nanometric spherical particles indicating the formation of globules or nanocrystalline apatite were observed on the surface of both bone scaffolds. This observation is supported by the qualitative results of the EDS analysis conducted on the sample surfaces. Fig. 7 shows the results of the EDS analysis taken from the sample surfaces. Intense peaks of Na and Cl were observed on the sample surfaces. This is attributed to the use of NaCl among the chemicals in the preparation procedure of the bioactive fluid and the adhesion of this salt to the sample surface. Additionally, besides the Na and Cl peaks,



(a) Viscosity (Pa.s) and Shear rate (s^{-1})

(b) G'- G" (Pa) ve time (s)

Fig. 5 Rheological values of the biomaterial

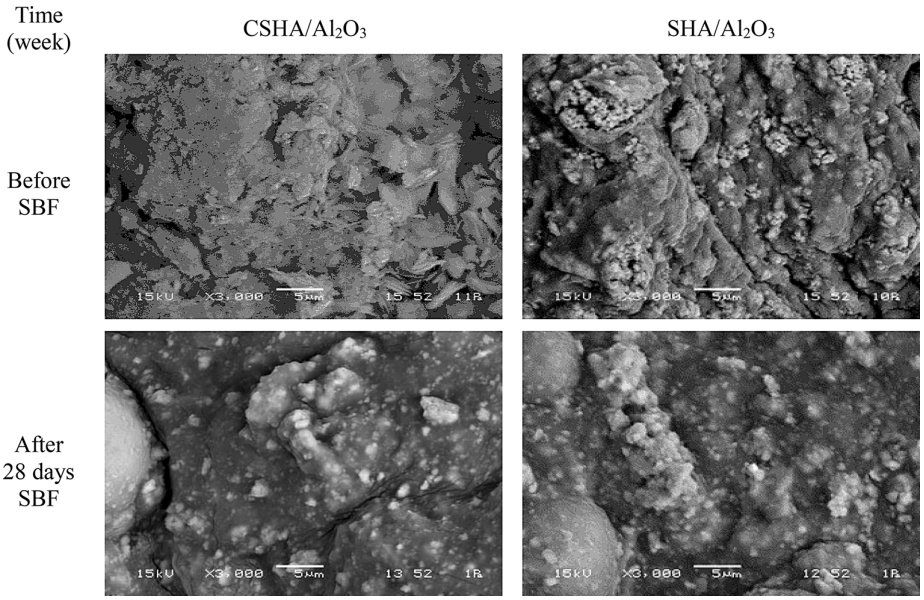
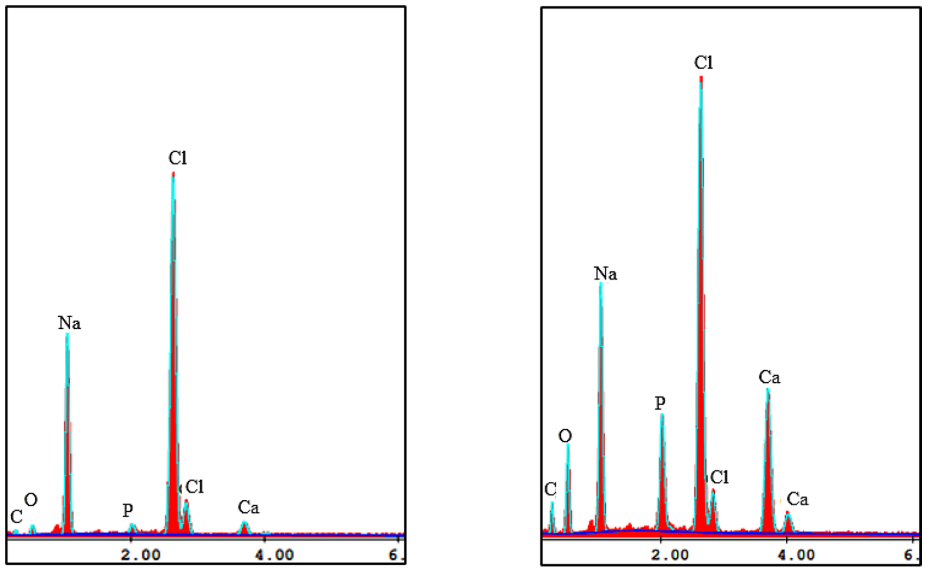


Fig. 6 SEM images of bone scaffolds after printing and after 28 days of soaking in SBF



(**a**) CSHA/ Al_2O_3 (**b**) SHA/ Al_2O_3

Fig. 7 EDS analysis of bone scaffolds after 28 days of immersion in SBF

significantly high peaks of Ca and P were observed, indicating the formation of an apatite layer on the surfaces of the samples soaked in SBF.

When examining the apatite nucleation based on the EDS results, the Ca/P ratio was calculated as 1.33 for the CSHA/ Al_2O_3 scaffold and 0.88 for the SHA/ Al_2O_3 scaffold. Thus, it was determined that the apatite nucleation was denser in the CSHA/ Al_2O_3 scaffold compared to the SHA/ Al_2O_3 scaffold (Table 2).

Fig. 8 shows the TF-FTIR spectrum of the apatite structure formed on the surface. Upon examination of the spectrum, an O-H stretching vibration is observed at 3698 cm^{-1}, carbonate groups are detected at 870 and 1612 cm^{-1}, and a PO_4^{3-} vibration band appears at 1005 cm^{-1}. The deposits have an apatite structure similar to bone. Obtained the values obtained are consistent with the results in the literature [32].

The quantitative evaluation method "TS EN ISO 10993-5/ October-2010-Annex C MTT Cytotoxicity Test" was used. The validity criteria for the test results obtained from the negative control and positive control should be above the specified threshold of 70%, as stated in the standard. Fig. 9 shows the viability values of L929 mouse fibroblast and osteoblast cell lines based on concentration.

Table 2 EDS spectra of the scaffold after 4 weeks of immersion

	Element	Weight [%]	Atomic [%]		Element	Weight [%]	Atomic [%]
CSHA/Al_2O_3	C	16.36	29.67	SHA/Al_2O_3	C	24.78	37.81
	O	8.21	11.18		O	26.24	30.05
	Na	38.44	36.43		Na	23.90	19.05
	P	1.38	0.97		P	5.31	3.14
	Cl	33.76	20.75		Cl	15.09	7.80
	Ca	1.84	1.00		Ca	4.69	2.14

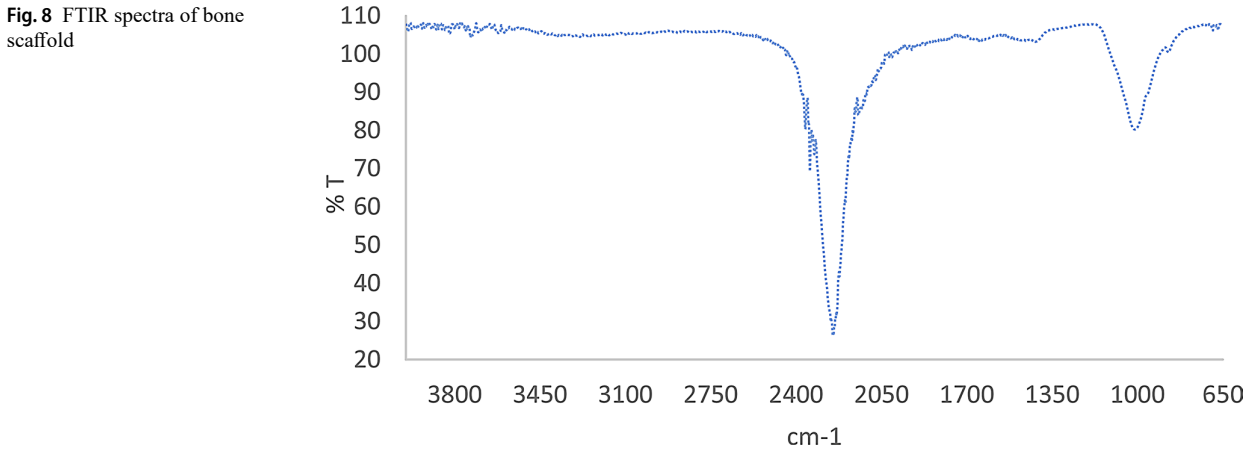


Fig. 8 FTIR spectra of bone scaffold

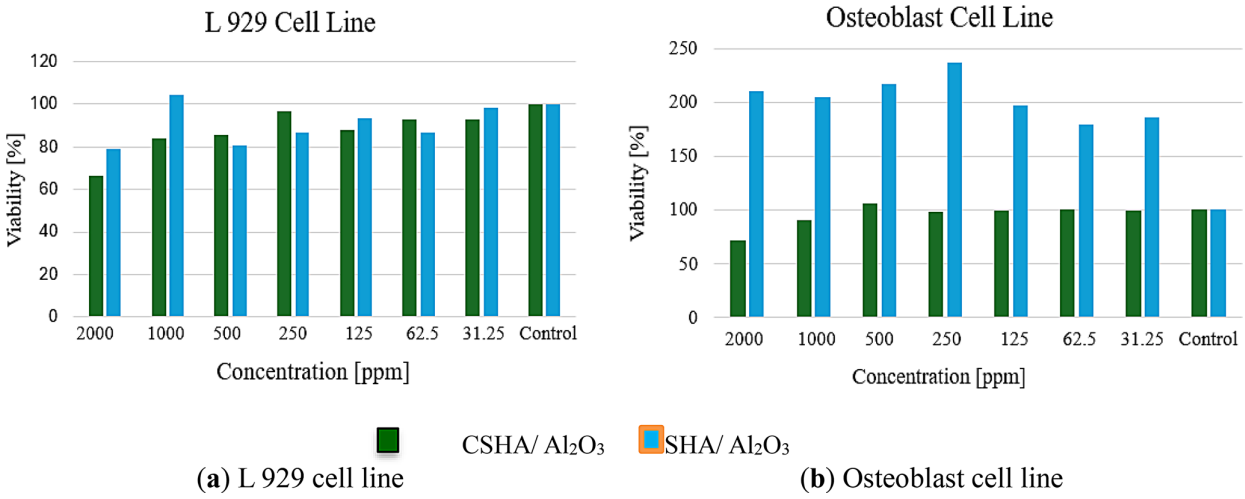


Fig. 9 Percentage viability graph of L929 mouse fibroblast and osteoblast cell lines based on concentration

Statistical analysis was performed using one-way analysis of variance (ANOVA) to examine the MTT analysis values in Fig. 9. MTT tests were conducted for 24 h. The statistical significance of live cells compared to control cells was.

determined. The critical value for statistical significance was defined as 0.05 [32].

The fibroblast cell line, there was no statistically significant difference between CSHA/ Al_2O_3 and SHA/ Al_2O_3 bone scaffold structures ($p > 0.05$). However, osteoblast cell line, there was a statistically significant difference between CSHA/ Al_2O_3 and SHA/ Al_2O_3 bone scaffold structures ($p < 0.05$).

Confocal microscope images of L929 mouse fibroblast cell line, DAPI, and MERGE for 12 and 36 h (0–50 µm) are presented in Fig. 10 [34].

After 12 h, similarities were observed in cell proliferation and network structure in both CSHA/ Al_2O_3 and SHA/ Al_2O_3 bone scaffold structures. However, upon examining

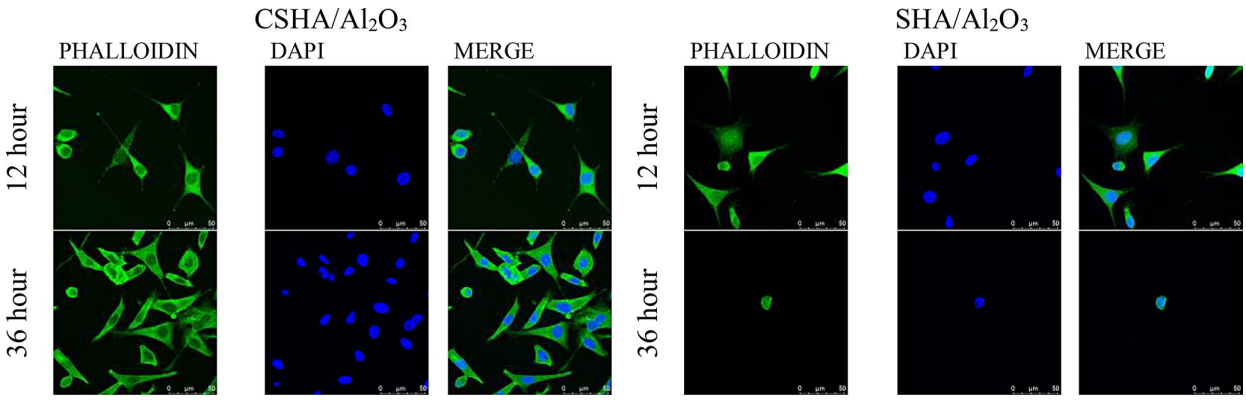


Fig. 10 Control group images of CSHA/ Al_2O_3 and SHA/ Al_2O_3 bone scaffold structures at 12 and 36 h in L929, DAPI, and MERGE confocal microscope

cell proliferation at 36 h, it was observed that cell proliferation continues in the CSHA/ Al_2O_3 bone scaffold.

Based on these results, the similarity in cell network structure and apatite formation in the CSHA/ Al_2O_3 bone scaffold has stabilized. It is anticipated that this developed biomaterial can be utilized in both in vivo and in vitro studies.

Discussion

The rheological behavior of the developed CSHA/Al_2O_3 and SHA/Al_2O_3-based bioinks exhibited a clear shear-thinning profile, which is a critical attribute for extrusion-based bioprinting. This property ensures smooth flow during deposition while promoting structural stability of the printed scaffolds. The observed decrease in viscosity with increasing shear rate and the absence of print failure (e.g., clogging, discontinuity) demonstrate the inks' reliable printability. These results align with prior studies on HA-based bioinks, which emphasized the significance of rheological tuning for ensuring both shape fidelity and extrusion precision [29, 33].

Additionally, the viscoelastic data showing G" > G' for both formulations confirm a predominance of viscous behavior, implying low internal cross-linking during the printing stage. This is advantageous for extrusion but suggests a need for post-print crosslinking strategies to improve construct stability, especially for long-term in vitro or in vivo applications. The comparable shear response of CSHA/Al_2O_3 and SHA/Al_2O_3 bioinks at higher shear rates (400–1000 s^{-1}) indicates similar extrusion dynamics, though the microstructural differences observed post-immersion suggest differences in biological behavior.

SEM analysis after 28 days of SBF immersion confirmed the formation of globular apatite structures on both scaffolds. When the 4 weeks SEM images are examined, it is seen that apatite formation in the bone tissue scaffold of CSHA/ Al_2O_3 (Ca 1.84 wt%) decreased compared to the bone scaffold of SHA/Al_2O_3 (Ca 4.69 wt%). The Ca/P ratio is calculated from the elemental composition (atomic percentages) obtained from EDS. These are calculated as CSHA/Al_2O_3 (1.33) and SHA/Al_2O_3 (0.88) (Table 2). The enhanced apatite nucleation may stem from the more favorable surface chemistry and microstructure of CSHA, consistent with earlier research showing the superior osteoconductive properties of synthetic HA- Al_2O_3 composites [35, 36]. Moreover, FTIR data revealed the presence of carbonate and phosphate groups characteristic of bone-like apatite, supporting the bioactive nature of the mineral phase.

Biocompatibility assessments further supported the material performance. MTT and WST-1 assays demonstrated > 70% cell viability in both L929 fibroblasts and osteoblasts, fulfilling ISO 10993-5 criteria. Interestingly, osteoblast proliferation was significantly higher on CSHA/Al_2O_3 scaffolds compared to SHA/Al_2O_3, indicating better support for osteogenic activity. This is likely attributed to CSHA's enhanced apatite content and more favorable microstructural features, including porosity and surface area, which are known to influence cell adhesion, proliferation, and differentiation [37].

Confocal microscopy revealed continued cell proliferation on CSHA/Al_2O_3 scaffolds at 36 h, suggesting enhanced cellular interactions and possible deeper cell infiltration. These findings imply that the scaffold architecture and bioactive surface chemistry effectively support not only initial cell attachment but also sustained metabolic activity and tissue ingrowth—both of which are critical for successful bone regeneration. However, certain limitations of this study must be acknowledged. First, while in vitro assays provide valuable insight, they do not fully replicate the complex physiological environment. Future work should include

in vivo studies to assess degradation, immunoresponse, and mechanical integration under load-bearing conditions. Furthermore, the mechanical performance of the scaffolds under dynamic stresses remains unexplored, which is essential for orthopedic applications.

In conclusion, the CSHA/Al_2O_3-based bioink demonstrated a superior combination of printability, bioactivity, and cytocompatibility, making it a promising candidate for bone tissue engineering. Continued research focused on mechanical reinforcement and in vivo validation is recommended to transition these materials toward clinical application.

Conclusions

In this study, composite bioinks formulated with synthetic and naturally derived HA combined with Al_2O_3 were systematically evaluated in terms of their rheological, morphological, and biological properties. Both CSHA/Al_2O_3 and SHA/Al_2O_3-based bioinks exhibited shear-thinning behavior, which is a desirable property for extrusion-based 3D bioprinting, enabling smooth flow and stable layer deposition.

SEM and EDS analyses confirmed the formation of apatite layers, particularly in the CSHA/Al_2O_3 scaffolds, following 28 days of immersion in simulated body fluid (SBF). The denser mineralization observed on these scaffolds highlights their superior bioactivity and osteoconductive potential. Furthermore, cell culture studies demonstrated that CSHA/Al_2O_3 scaffolds promoted greater osteoblast proliferation and adhesion compared to SHA/Al_2O_3, likely due to their enhanced surface characteristics and mineral content.

These findings suggest that CSHA/Al_2O_3-based bioinks possess a favorable combination of printability, biocompatibility, and mineralization capacity, positioning them as strong candidates for bone tissue engineering applications. However, further in vivo studies are recommended to evaluate long-term biological and mechanical behavior under physiological conditions. Such investigations will be crucial for the clinical translation of these hybrid bioinks into regenerative medicine practices.

Acknowledgements All authors thank the Kocaeli University Stem Cell Center, where cell cultures were performed and Hitit University Scientific Research Projects Coordinatorship (HUBTUAM).

Author contributions Nermin Demirkol- Rheology analyses, cell tests, study planning, Aysu Akilli Ari- scaffold production, composite bioink preparation, bioprinting design, Hatice Evlen- bioprinting, study planning, mechanical tests, cell tests.

Funding Open access funding provided by the Scientific and Technological Research Council of Türkiye (TÜBİTAK). Scientific Research Project Department of Karabuk University for financial support as part of the KBÜBAP-17-DR-303 project.

Data availability All data within the manuscript. No more additional data is available.

Declarations

Ethical approval Not applicable.

Competing interests The authors declare no competing interests.

Open Access This article is licensed under a Creative Commons Attribution 4.0 International License, which permits use, sharing, adaptation, distribution and reproduction in any medium or format, as long as you give appropriate credit to the original author(s) and the source, provide a link to the Creative Commons licence, and indicate if changes were made. The images or other third party material in this article are included in the article's Creative Commons licence, unless indicated otherwise in a credit line to the material. If material is not included in the article's Creative Commons licence and your intended use is not permitted by statutory regulation or exceeds the permitted use, you will need to obtain permission directly from the copyright holder. To view a copy of this licence, visit http://creativecommons.org/licenses/by/4.0/.

References

1. Sadeghinia, A., Davaran, S., Salehi, R., Jamalpoor, Z.: Nano-hydroxy apatite/ chitosan/gelatin scaffolds enriched by a combination of platelet-rich plasma and fibrin glue enhance proliferation and differentiation of seeded human dental pulp stem cells. Biomed. Pharmacother. **109**, 1924–1931 (2019). https://doi.org/10.1016/j.biopha.2018.11.072
2. Jones, A.C., Arns, C.H., Sheppard, A.P., Hutmacher, D.W., Milthorpe, B.K., Knackstedt, M.A.: Assessment of bone ingrowth into porous biomaterials using MICRO-CT. Biomaterials. **28**, 2491–2504 (2007). https://doi.org/10.1016/j.biomaterials.2007.01.046
3. Meyer, U.: The history of tissue engineering and regenerative medicine in perspective. In: Fundamentals of Tissue Engineering and Regenerative Medicine. Springer. (2009). https://doi.org/10.1007/978-3-540-93961-5_1
4. Sallent, I., Capella-Monsonís, H., Procter, P., Bozo, I.Y., Deev, R.V., Zubov, D., Vasyliev, R., Perale, G., Pertici, G., Baker, J.: The few who made it: Commercially and clinically successful innovative bone grafts. Front. Bioeng. Biotechnol. **8**, 952 (2020). https://doi.org/10.3389/fbioe.2020.00952
5. Tang, G., Liu, Z., Liu, Y., Yu, J., Wang, X., Tan, Z., Ye, X.: Recent trends in the development of bone regenerative biomaterials. Front. Cell. Dev. Biol. **9**, 665813 (2021). https://doi.org/10.3389/fcell.2021.665813
6. Wang, W., Yeung, K.W.: Bone grafts and biomaterials substitutes for bone defect repair: A review. Bioact Mater. **2**, 224–247 (2017). https://doi.org/10.1016/j.bioactmat.2017.05.007
7. Rupp, M., Klute, L., Baertl, S., Walter, N., Mannala, G.K., Frank, L., Pfeifer, C., Alt, V., Kerschbaum, M.: The clinical use of bone graft substitutes in orthopedic surgery in Germany—a 10-years survey from 2008 to 2018 of 1,090,167 surgical interventions. J. Biomed. Mater. Res. B Appl. Biomater. **110**, 350–357 (2022). https://doi.org/10.1002/jbm.b.34911
8. Koons, G.L., Diba, M., Mikos, A.G.: Materials design for bone-tissue engineering. Nat. Rev. Mater. **5**, 584–603 (2020). https://doi.org/10.1038/s41578-020-0209-1
9. Sahebalzamani, M., Ziminska, M., Mccarthy, H.O., Levingstone, T.J., Dunne, N.J., Hamilton, A.R.: Advancing bone

tissue engineering one layer at A time: A layer-by-layer assembly approach to 3D bone scaffold materials. Biomater. Sci. **10**, 2734–2758 (2022). https://doi.org/10.1039/D1BM01756J
10. Bahraminasab, M.: Challenges on optimization of 3D-printed bone scaffolds. Biomed. Eng. Online. **19**, 1–33 (2020). https://doi.org/10.1186/s12938-020-00810-2
11. Shi, Q., Shui, H., Chen, Q., Li, Z.-Y.: How does mechanical stimulus affect the coupling process of the scaffold degradation And bone formation: An in Silico approach. Comput. Biol. Med. **117**, 103588 (2020). https://doi.org/10.1016/j.compbiomed.2019.103588
12. Park, S.-H., Gil, E.S., Shi, H., Kim, H.J., Lee, K., Kaplan, D.L.: Relationships between degradability of silk scaffolds and osteogenesis. Biomaterials. **31**, 6162–6172 (2010). https://doi.org/10.1016/j.biomaterials.2010.04.028
13. Sharma, A., Molla, M.S., Katti, K.S., Katti, D.R.: Multiscale models of degradation and healing of bone tissue engineering nanocomposite scaffolds. J. Nanomechan Micromechan. **7**, 04017015 (2017). https://doi.org/10.1061/(ASCE)NM.2153-5477.0000133
14. Zhang, H., Zhou, L., Zhang, W.: Control of scaffold degradation in tissue engineering: A review. Tissue Eng. B Rev. **20**, 492–502 (2014). https://doi.org/10.1089/ten.teb.2013.0452
15. Cavallo, A., Al Kayal, T., Mero, A., Mezzetta, A., Guazzelli, L., Soldani, G., Losi, P.: Fibrinogen-Based Bioink for application in skin equivalent 3D Bioprinting. J. Funct. Biomaterials. **14**(9), 459 (2023). https://doi.org/10.3390/jfb14090459
16. Silva-Holguin, P.N., de Jesús Ruíz-Baltazar, Á., Reyes-López, S.Y.: Antimicrobial study of the Al_2O_3-Cu and Al_2O_3-Hydroxiapatite-Cu spheres. Inorg. Chem. Commun. **138**, 109253 (2022). https://doi.org/10.1016/j.inoche.2022.109253
17. Tajvar, S., Hadjizadeh, A., Samandari, S.S.: Scaffold degradation in bone tissue engineering: An overview, International Biodeterioration & Biodegradation, Volume 180, 105599, ISSN 0964–8305, (2023). https://doi.org/10.1016/j.ibiod.2023.105599
18. Verma, R., Mishra, S.R., Gadore, V., Ahmaruzzaman, M.: Hydroxyapatite-based composites: Excellent materials for environmental remediation and biomedical applications. Adv. Colloid Interface Sci. 102890 (2023). https://doi.org/10.1016/j.cis.2023.102890
19. Ferraz, M.P., Monteiro, F.J., Manuel, C.M.: Hydroxyapatite nanoparticles: A review of Preparation methodologies. J. Appl. Biomaterials Biomech. **2**(2), 74–80 (2004). https://doi.org/10.1177/228080000400200202
20. Thian, E.S., Konishi, T., Kawanobe, Y., Lim, P.N., Choong, C., Ho, B., Aizawa, M.: Zinc-substituted hydroxyapatite: A biomaterial with enhanced bioactivity and antibacterial properties. J. Mater. Science: Mater. Med. **24**, 437–445 (2013). https://doi.org/10.1007/s10856-012-4817-x
21. Motameni, A., Çardaklı, İ.S., Gürbüz, R., Alshemary, A.Z., Razavi, M., Farukoğlu, Ö.C.: Bioglass-polymer composite scaffolds for bone tissue regeneration: A review of current trends. Int. J. Polym. Mater. Polym. Biomaterials. 1–20 (2023). https://doi.org/10.1080/00914037.2023.2186864
22. Gudkov, S.V., Burmistrov, D.E., Smirnova, V.V., Semenova, A.A., Lisitsyn, A.B.: A Mini Review of Antibacterial Properties of Al_2O_3 Nanoparticles. Nanomaterials 2022, 12, 2635. (2022). https://doi.org/10.3390/nano12152635
23. Lavagnini, I.R., Campos, J.V., Osiro, D., Ferreira, J.A., Colnago, L.A., Pallone, E.M.: Influence of alumina substrates open porosity on calcium phosphates formation produced by the biomimetic method. Prog. Biomater. **11**(3), 263–271 (2022). https://doi.org/10.1007/s40204-022-00193-8
24. Anna, P., Jana, V., Milan, P., Peter, Š., František, Š., Aydar, R.,… Dušan, G. (2023).Structure, thermal properties and crystallization behavior of binary Y2O3–Al2O3 glasses with high alumina content. Journal of Materials Research and Technology,26, 2333–2351. https://doi.org/10.1016/j.jmrt.2023.08.067.
25. Demirkol, N., University, I.T.: Institute of Science and Technology, Department of Metallurgical and Materials Engineering, PhD thesis, (2013)
26. Ari, A.A., Evlen, H., Demirkol, N.: Biological and morphological effects of apatite kinds (Sheep/Synthetic) on MgO reinforced bone tissue with hydroxyapatite matrix. Acta Phys. Pol. A., **142**(2) (2022). https://doi.org/10.12693/APhysPolA.142.201
27. Ahmet, P.A.S.İ.N.L.İ., Sami, R.: AKSOY, Yapay Kemik Uygulamaları İçin hidroksiapatit. BiyoTeknoloji Elektronik Dergisi Cilt: 1 No 1, (41–51). (2010)
28. Sanz-Garcia, E.S.-O.A.: Alpha Pernia-Espinoza and Carmen Escobedo-Lucea, Accurate Calibration in Multi-Material 3D Bioprinting for Tissue Engineering, Materials 2018, 11, 1402; doi:10.3390/ma11081402, Materials 11, 1402). (2018). https://doi.org/10.3390/ma11081402
29. Groll, J., Burdick, J.A., Cho, D.W., Derby, B., Gelinsky, M., Heilshorn, S.C., Jüngst, T., Malda, J., Mironov, V.A., Nakayama, K., Ovsianikov, A., Sun, W., Takeuchi, S., Yoo, J.J., Woodfield, T.B.F.: A definition of Bioinks and their distinction from biomaterial inks. Biofabrication. A., **8**(1), 013001 (2016). https://doi.org/10.1088/1758-5090/8/1/013001
30. Malda, J., Visser, J., Melchels, F.P.W., Jüngst, T., Hennink, W.E., Dhert, W.J.A., Groll, J., Hutmacher, D.W.: 25th anniversary article: Engineering hydrogels for biofabrication. Adv. Mater. A., **25**(36), 5011–5028 (2013). https://doi.org/10.1002/adma.201302042
31. Ozbolat, I.T.: 3D Bioprinting: Fundamentals, Principles and Applications. Academic (2016)
32. Ari, A.A., University, K.: Institute of Natural and Applied Sciences, Department of Industrial Design Engineering, PhD thesis, (2022)
33. Ribeiro, A., Blokzijl, M.M., Levato, R., Visser, C.W., Castilho, M., Hennink, W.E., Vermonden, T., Malda, J.: Assessing Bioink shape fidelity to aid material development in 3D Bioprinting. Biofabrication. A., **10**(1), 014102 (2018). https://doi.org/10.1088/1758-5090/aa90e2
34. Çelik, A.C.T., Kölüş, T.: 3 Farkli dentin Hassasiyeti giderici diş Macununun Sitotoksisitesinin değerlendirilmesi. Selcuk Dent. J. A., **8**(2), 460–466 (2021). https://doi.org/10.15311/selcukdentj.696055
35. Lavagnini, I.R., Campos, J.V., Osiro, D., Ferreira, J.A., Colnago, L.A., Pallone, E.M.: Influence of alumina substrates open porosity on calcium phosphates formation produced by the biomimetic method. Prog. Biomater. A., **11**(3), 263–271 (2022). https://doi.org/10.1007/s40204-022-00193-8
36. Kim, H.W., Knowles, J.C., Kim, H.E.: Hydroxyapatite and alumina composites for biomedical applications. Biomaterials. A., **27**(36), 5784–5793 (2016). https://doi.org/10.1016/j.biomaterials.2006.07.028
37. Koons, G.L., Diba, M., Mikos, A.G.: Materials design for bone-tissue engineering. Nat. Reviews Mater. A., **5**, 584–603 (2020). https://doi.org/10.1038/s41578-020-0209-1

Publisher's note Springer Nature remains neutral with regard to jurisdictional claims in published maps and institutional affiliations.